Abdelrazek *et al.*
Journal of Engineering and Applied Science (2022) 69:103
https://doi.org/10.1186/s44147-022-00158-5

Journal of Engineering and Applied Science

RESEARCH Open Access

Piston bowl shape and biodiesel fuel effects on combustion and emission of diesel engines

Mohamed Khaled Abdelrazek*, Mohsen Mohamed Abdelaal and Ahmed Mustafa El-Nahas

*Correspondence: eng.mohammadkh94@gmail.com

Department of Mechanical Engineering, Faculty of Engineering, Al-Azhar University, Cairo 11371, Egypt

Abstract

This study aims to investigate the effects of piston bowl shape and biodiesel fuel on combustion and emissions of a direct injection (DI) diesel engine. Three configurations of piston bowl geometry are modeled: hemispherical, toroidal, and rectangular. Biodiesel fuel derived from soybean oil is being considered. An experimental work was conducted on a diesel engine with a hemispherical piston bowl, and a better validity was attained. The study showed that, diesel engine with toroidal piston bowl delivered the largest power than other shapes, where turbulent regions are formed inside the toroidal piston bowl with higher intensity, which resulted in better combustion characteristics and lower emission concentrations. It is observed from the combustion of biodiesel fuel that, the rapid combustion stage began earlier than conventional diesel fuel by about 5^{o} CA, heat release rate (HRR) decreased by 18.88%, emissions of carbon monoxide (CO), and unburnt hydrocarbon (UHC) reduced but nitric oxide (NO) emission increased by about 17.78% at 55^{o} CA, as compared to diesel fuel. During the injection process, the jet core of biodiesel fuel appeared thicker and longer than conventional diesel fuel. For optimization, preheating with exhaust gas recirculation (EGR) of biodiesel fuel contributes to reduce the emissions of nitrogen oxides (NO_x) and improve the atomization rate.

Keywords: Piston bowl shape, Biodiesel, Diesel engine, Combustion, Emission

Introduction

The demand for diesel engines will rise as they contribute to serve more sectors such as transportation, logistics activities in industry, and power plants. Due to the high demand for diesel engines, there are anticipated concerns about the increase in the proportion of harmful emissions into the atmosphere, so searching for new strategies to develop and improve the engine performance has become mandatory and urgent. Emission percentage and combustion efficiency in diesel engines are affected by several parameters such as air to fuel ratio, compression ratio, air and fuel preheating, fuel blends, combustion chamber geometry, injection timing, injection pressure, and exhaust gas recirculation (EGR). Studying the mentioned parameters at different operating conditions experimentally is costly and time-consuming. Modeling using computational fluid dynamics (CFD) is considered beneficial and effective, which facilitates and speed up the process of engine assessment when changing parameters [1–4].

In the past decades, researchers have conducted many studies to improve diesel engine performance. Jayashankara et al. [5] conducted a CFD study on the effect of injection timing and intake pressure on a direct injection diesel engine. Zhijun Peng et al. [6] investigated numerically a multi-pulse injection strategy for premixed charge compression ignition (PCCI) combustion in a direct injection diesel engine, and reported that the emission formation and combustion inside the diesel engine are significantly influenced by the injection timing and fuel splitting proportion. Abdul Gafoor et al. [7] investigated the effect of initial swirl ratio and piston bowl geometry on a diesel engine performance using a CFD code. A rectangular piston bowl was the considered piston bowl shape in their study where they changed the bowl diameter and the corresponding swirl ratio more than once to examined the effect on emission and combustion characteristics. This study reported that a large swirl ratio with high turbulent kinetic energy (TKE) is important to improve the combustion efficiency. Rakopoulos et al. [8] conducted a numerical simulation on the effects of speed and piston bowl geometry in a motored diesel engine and reported that the engine performance is greatly influenced by the in-cylinder gas flow, injection pressure and the geometry of the combustion chamber. Jaichandar et al. [9] investigated experimentally the effects of combustion chamber geometry and injection timing on a diesel engine fueled with biodiesel fuel and concluded that the piston bowl geometry contributed to the improvement of engine performance and the biodiesel fuel resulted in a high NO_x emission. Saito et al. [10] studied the effects of combustion chamber geometry on combustion characteristics of a DI diesel engine and reported that a re-entrant combustion chamber improved the combustion efficiency due to the higher turbulent flow velocity, which resulted in lower levels of soot inside the engine cylinder. Rajamani et al. [11] carried out a CFD simulation of the effect of piston bowl geometry and the nozzle configuration on a combustion system with an optimization on re-entrant piston bowl geometry. Previous works show that the piston bowl geometry significantly affects the diesel engine performance.

Several studies have discussed the effect of fuel type on diesel engine performance. Biodiesel fuel is the most common fuel that considered for study because it is a biodegradable and renewable fuel and is considered environmentally friendly [12]. Biodiesel fuel sources may be vegetable oils or animal fats. Biodiesel fuel is produced by a common method, namely transesterification. Through this method, a chemical reaction takes place between the oil and alcohol in the presence of a catalyst, and the reaction results in fatty acid methyl esters (FAMES) and glycerol. Figure 1 shows the transesterification reaction of triglyceride (vegetable oil) with methanol alcohol in the presence of potassium hydroxide. The chemical and physical properties of biodiesel fuel are different from conventional diesel fuel, this difference will have a significant impact on the combustion and emission within the diesel engine [13, 14]. Climate change, rising crude oil prices, energy security, and increased air population have prompted the scientific society to look for alternatives to conventional fossil fuels [15, 16]. Biodiesel fuel derived from various sources, including jatropha, pongamia, mahua, and nerium, was investigated in India [17]. Kiat Ng et al. [18] carried out a numerical investigation of the effects of three types of biodiesel fuels on a DI diesel engine performance and concluded that the combustion of biodiesel fuel is significantly influenced by the physical and chemical properties of the fuel, especially the proportion of unsaturated fatty acids. Bai-Fu Lin

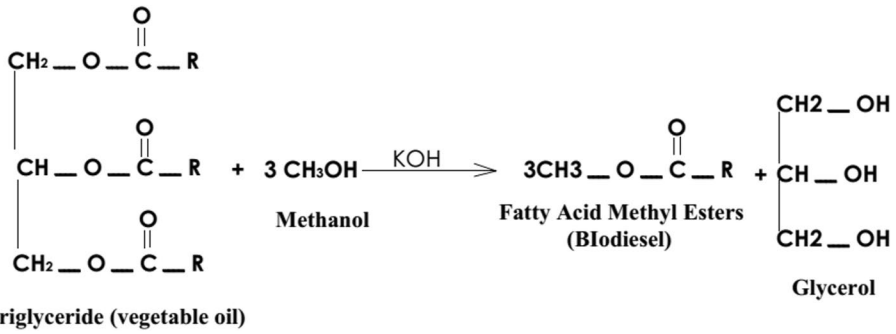

Fig. 1 Transesterification reaction

et al. [19] studied the effects of eight types of biodiesel fuels on a DI diesel engine and reported that the biodiesel fuel achieves a significant increase in brake specific fuel consumption (BSFC) as well as an increase in NO_x emissions compared to conventional diesel fuel. Canakcı M [20] studied the effect of soybean biodiesel fuel and its blends with conventional diesel fuel on a diesel engine performance and concluded that all blends of biodiesel provided a reduction in particulate matter (PM), hydrocarbon (HC) and carbon monoxide (CO) emissions except NO_x. Previous studies agreed that biodiesel fuel positively affects the diesel engine by reducing the proportion of harmful emissions, meanwhile having a negative effect on the engine performance, such as increasing the NO_x emissions and decreasing the engine torque. In the recent years, researchers have moved toward the study of biodiesel combustion improvement. EL-Seesy et al. [21] conducted an experimental study on the improvement of combustion and emissions of a diesel engine fueled with diesel/jojoba oil blends and butanol additive and concluded that the addition of butanol to the blends results in an increase in peak pressure and heat release rate inside the engine cylinder, whereas the NO_x, CO, and HC emissions are reduced. Senthilkumar et al. [22] carried out a study of the effect of diesel-waste plastic oil on a single cylinder, 4-stroke, DI diesel engine performance and emissions. This study reported that the increase of the biodiesel in fuel blends reduces the thermal efficiency and the emissions of CO and HC, but the NO_x emissions increase. Sivakandhan et al. [23] conducted an experimental investigation on a diesel engine fueled with sardine oil methyl ester and diesel fuel with manganese oxide (MnO_2) nanoparticles and reported that the MnO_2 additives improved the engine performance and reduced the emissions.

The main objective of the present work is to analyze the effects that result from the use of three configurations of piston bowl geometry; hemispherical, toroidal and rectangular on a DI diesel engine, in addition to study the effects resulting from the use of biodiesel fuel that is derived from soybean oil.

Experimental methodology

The present work was conducted on a direct injection, four-stroke, water cooled, naturally aspirated, single cylinder diesel engine. Table 1 shows the diesel engine specifications. A direct current (DC) universal dynamometer is coupled to the crank shaft of the diesel engine and can be used as a motor to drive the engine at the start or as a generator to absorb the output power from the engine. The dynamometer rotor it

Table 1 Engine specifications

Engine model	Petter PH1W
No. of cylinder	1
Bore × stroke (mm)	87.3 × 110
Displacement (cm^3)	659
Compression ratio	16.5:1
Speed (rpm)	1500
Connecting rod Length (mm)	192.5
Max. power (kw)	5.07 kw at 1500 rpm
Max. torque (Nm)	25 Nm at 1500 rpm
Intake valve closing IVC	35.5° aBDC
Exhaust valve opening EVO	35.5° bBDC

coupled to the engine crank shaft and rotate at the same speed of the engine. The dynamometer housing is free to turn but it is restricted by a torque arm of 25 cm and connected to a spring scale. The dynamometer housing attempts to turn when the engine is loaded due to the generated electromagnetic field. By increasing the engine load, the field strength increases and the spring scale indicates the force (F) exerted by the housing in Newtons (N). A magnetic tachometer device is used to measure the rotational speed (ω) of the engine. The engine power is determined by the following equation:

$$\text{Engine Power} = 0.25(\text{F}\ \omega)$$

The exhaust gas temperature is measured by a type K thermocouple, which has a sensitivity of 41 μV/°C and standards error of ± 2.2 °C. The inlet air mass flow rate is measure by an orifice mounted on a damping reservoir and an inclined manometer installed underside the damping reservoir to indicate the pressure difference across the orifice in mm H_2O. The inlet air mass flow rate ($\dot{m}_{air}$) is determined by the following equation:

$$\dot{m}_{\text{air}} = \text{K}\sqrt{\text{h}}$$

Where K is a constant and its value is based on the test conditions, the considered value of K was 5.902, h is a manometer reading in mm H_2O. The fuel mass flowrate ($\dot{m}_{fuel}$) is determined as

$$\dot{m}_{\text{fuel}} = \frac{\rho \text{V}}{t}$$

Where t is the time during which a certain volume (V) of fuel is consumed, ρ is the fuel density. The pressure inside the engine cylinder is measured by a Piezoelectric sensor, which has a measurement limit up to 206.85 bar and a sensitivity of 1 pC/psi. Once the pressure inside the engine rises, the Piezoelectric sensor sends a signal through a high temperature coaxial cable to a dual mode charge amplifier, which has a limit up to 100,000 pC of the input charge, a converting range from 0.1 to 10,000 mV/pC, and an output range of ± 10 V. The output signal from the amplifier is directly

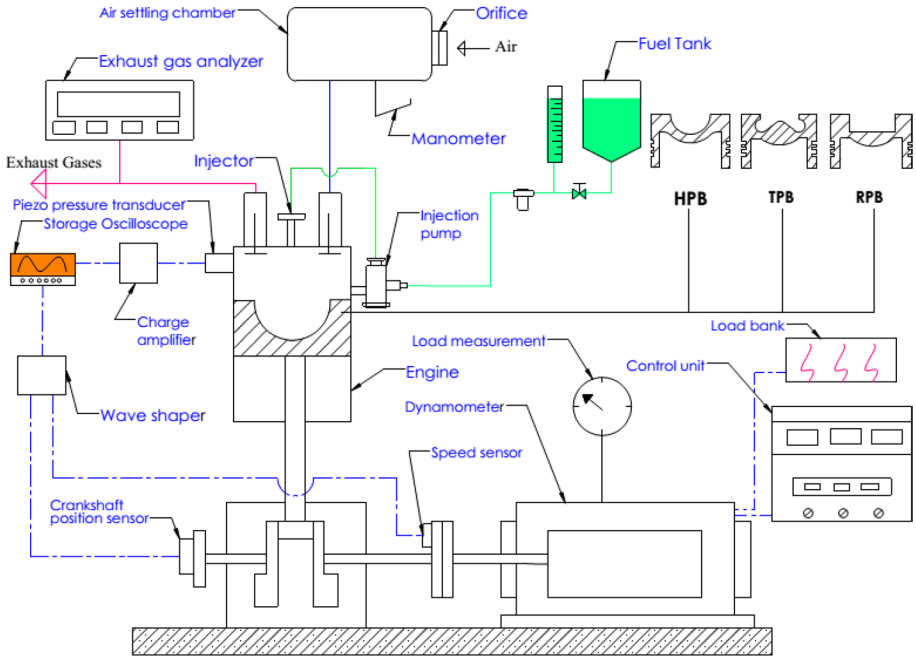

Fig. 2 Engine test bench

Table 2 Accuracy and uncertainty of measured parameters

Measured parameter	Accuracy	Uncertainty (%)
Air flow rate	±0.2 mm H2O	1.64
Diesel fuel flow rate	$\pm 8.27 \times 10^{-3}$ kg/h	1.51
Engine brake power	±0.15 kW	2.9
In-cylinder pressure	±2%	4.92
Crankshaft position	±1%	3.9
NO	±5 ppm	5.88
CO	±1%	3.28
HC	±3 ppm	3.08

transferred to a two-channel storage oscilloscope through a coaxial cable for analysis and recording. An ADC gas analyzer, model MGA3000, was used to measure the exhaust emissions of the combustion process. This model is capable of measuring the concentration of CO, CO_2, NO, HC, and O_2 emissions. These emissions have been measured based on the non-dispersive infrared principle, the paramagnetic principle and the flame ionization detector. Figure 2 shows the engine test bench. Accuracies and uncertainties of the measured parameters are given in Table 2.

Numerical method

Closed cycle simulation method is employed in the present study, during which the diesel engine simulation starts from the point of intake valve closure to the point of exhaust valve opening. Due to the symmetry of the engine cylinder and fuel injector,

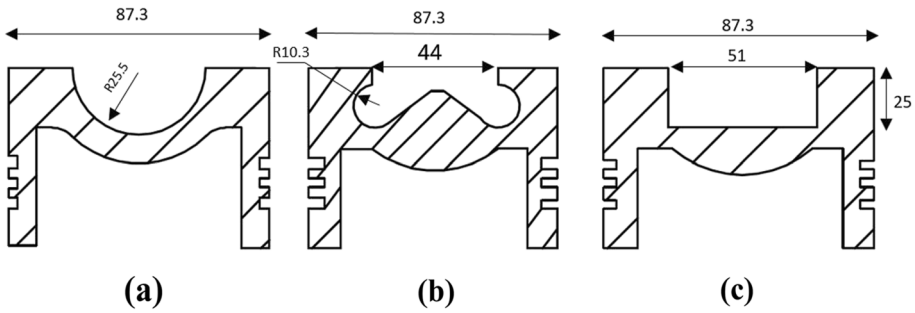

Fig. 3 **a** Hemispherical, **b** toroidal, and **c** rectangular piston bowl

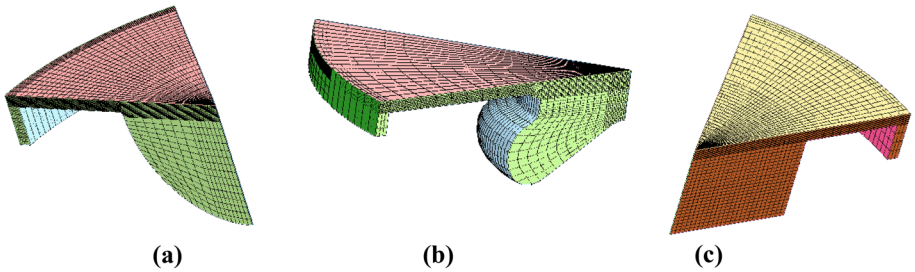

Fig. 4 Sector mesh of **a** hemispherical, **b** toroidal, and **c** rectangular piston bowl geometry

the piston geometry is divided into sectors in order to reduce computational time. One eighth sector is used to represent the computational domain.

Figure 3 depicts three configurations of piston bowl geometry, which are hemispherical, toroidal, and rectangular. The hexahedron mesh is generated through a commercial CFD code with a cell height of 1.6 mm, the cell expansion ratio from piston was 1.01 and the cell expansion ratio from head was 1.01 (see Fig. 4). According to the spherical coordinate system, the nozzle direction angles are set to $\theta = 42^{o}$ and $\phi = 22.5^{o}$, as shown in Fig. 5. Boundary and initial conditions are given in Table 3.

The tested fuels are diesel and soybean biodiesel fuels and their physical and chemical properties are tabulated in Tables 4 and 5, according to European Union EN 590 and EN 14214 standards. Biodiesel fuel contains saturated and non-saturated fatty acid methyl esters and the proportion of these acids affects the chemical and physical properties of the fuel and, therefore, will significantly affect the combustion of biodiesel fuel. Table 6 shows the saturated and non-saturated fatty acid methyl esters content in soybean biodiesel fuel.

For fuels chemistry, n-heptane reaction mechanism by [24] is used as a surrogate fuel model to represent the chemical kinetics of the diesel fuel and for the soybean biodiesel fuel, a combination of methyl decanoate MD, methyl-9-decanoate MD9D and n-heptane is used as a reaction mechanism to represent the saturated and non-saturated of the oxygenated hydrocarbon chain of biodiesel fuel, which includes 247 species and 1129 reactions [25].

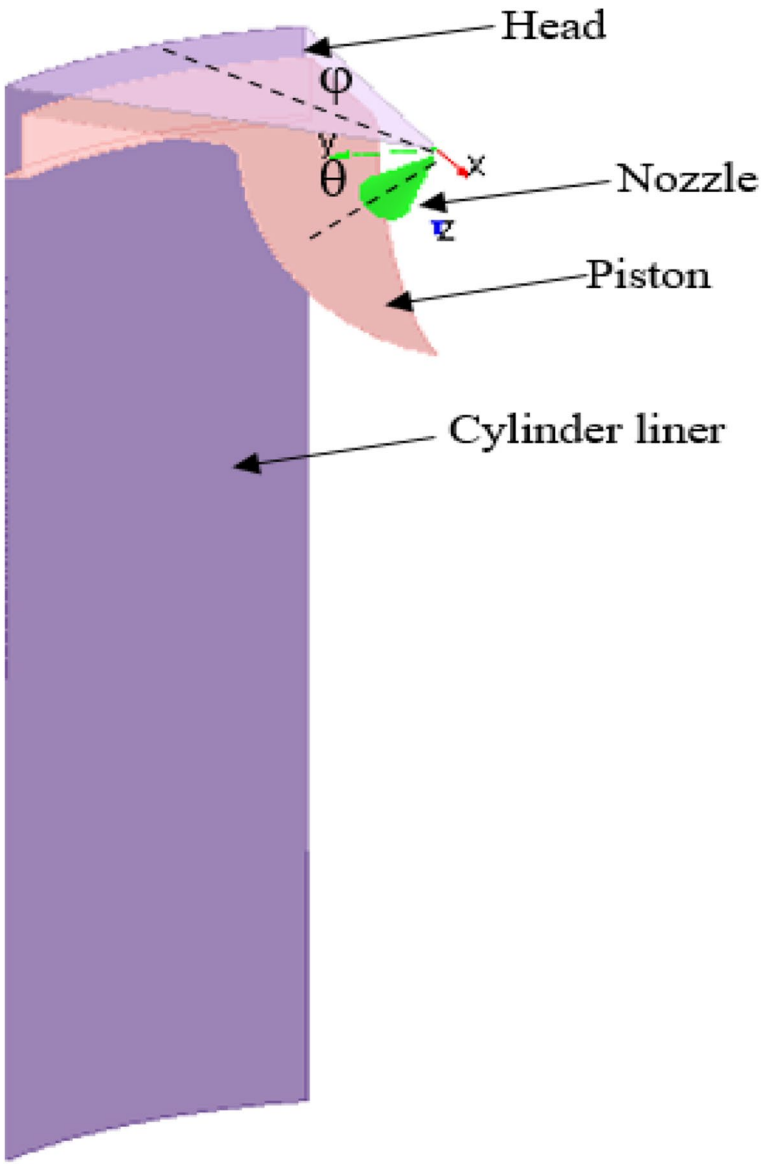

Fig. 5 Model configuration

Table 3 Boundary and initial conditions

Head temperature (K)	470
Liner temperature (K)	420
Piston temperature (K)	500
Initial pressure (bar)	1
Initial temperature (K)	370
Injected fuel mass (mg/cycle)	7.03
Inflow droplet temperature (K)	320
Start of injection	17 CA bTDC
Injection duration (CA)	15
Initial swirl ratio	1.5

Table 4 Conventional diesel fuel properties

Specification	Test method	Test results
Typical formula		C14.16H25.21
Average molecular weight (g/kmol)		195.5
Lower heating value (MJ/kg)		42.93
Density at 15 °C (kg/m^3)	EN ISO 3675, EN ISO 12185	838
Flash point (°C)	EN ISO 2719	64
Sulfur content (mg/kg)	EN ISO 8754	2117
Cetane index	EN ISO 4264	53.8
Kinematic Viscosity 40 °C (mm^2/s)	EN ISO 3104	2.317
Ash content (wt%)	EN ISO 6245	0.0063
Polycyclic aromatic hydrocarbons (wt%)	EN ISO 12196	7

Table 5 Soybean biodiesel fuel properties

Specification	Units	Test method	EN 14214 limits		Test results
			Min.	Max.	
Typical formula					C18.74H34.51O2
Average molecular weight	g/kmol				291.2
Lower heating value	MJ/kg				37.4
Density at 15 °C	kg/m^3	EN ISO 12185	____	900	883.4
Flash point	°C	EN ISO 3679	120	____	123
Sulfur content	mg/kg	EN ISO 20884	____	10	1.3
Cetane index		EN ISO 5165	51	____	54.1
Kinematic viscosity 40 °C	mm^2/s	EN ISO 3104	3.5	5	4.512
Cold filter plugging point	°C	EN 116	____	+ 5 °C (summer) – 15 °C (winter)	– 18
Water content	mg/kg	EN ISO 12937	____	500	357
Oxidation stability at 110 °C	Hours	EN 14112	6	____	7.1
Acid value	mg KOH/g	EN 14104	____	0.5	0.36
Iodine value	g Iodine/100 g	EN 14111	____	120	115
Methanol content	wt%	EN 14110	____	0.2	0.11
Free glycerin	wt%	EN 14111	____	0.02	0.01
Monoglyceride content	wt%	EN 14105	____	0.8	0.5
Diglyceride content	wt%	EN 14105	2	0.2	0.12
Triglyceride content	wt%	EN 14105	____	0.2	0.16

Table 6 Fatty acid methyl esters FAMEs content in soybean biodiesel fuel

Fatty acid	Relative percentage
Methyl palmitate (C16:0)	9.4
Methyl stearate (C18:0)	4.1
Methyl oleate (C18:1)	22
Methyl linoleate (C18:2)	55.3
Methyl linolenate (C18:3)	8.9

Models and validation

The models used to describe the reaction mechanism of both diesel and biodiesel fuel are n-heptane and a combination of methyl decanoate MD, methyl-9-decanoate MD9D and n-heptane, heir details, and validation are available in the literature [24, 25].

A solid cone injector is used in the present study where the spray atomization and droplet breakup are modeled by the Kelvin-Helmholtz/Rayleigh-Taylor (KH/RT) hybrid model. The solid cone spray is divided into two zones, the first one starting from the nozzle exit and during which the fuel jet still dense but some droplets leave the jet, this zone is associated by Kelvin-Helmholtz modeling. At the end of the first zone, the fuel jet turns into small droplets, this zone is associated by Rayleigh-Taylor modeling, details and validation are available in [26, 27]. When the spray droplets impinge on wall surface, this impingement will result in the occurrence of sticking, rebound, spread or splashing (see Fig. 6), and this is determined by the Reynolds number and Weber number [28], as follows:

1. Stick $We_n \leq 5$
2. Rebound $5 < We_n \leq 10$
3. Spread $We_n > 10$ and $We_n\, Re_n^{0.5} < H_{cr}$
4. Splash $We_n\, Re_n^{0.5} \geq H_{cr}$

$$We_n = \frac{\rho U^2 D}{\sigma},\ Re_n = \frac{\rho U D}{\mu},\ \text{and}\ H_{cr} = [1500 + \frac{650}{\beta^{0.42}}][1 + 0.1 Re_n^{0.5} \text{mim}(\delta, 0.5)]$$

Where We_n is the Weber number, Re_n is the Reynolds number, ρ is the liquid density, U is the normal velocity of the droplet to the impact surface, D is the droplet diameter, σ is the surface tension, μ is the liquid viscosity, β is the roughness height to incident droplet diameter ratio, δ is the film thickness to incident droplet diameter ratio and H_{cr} is the splash threshold proposed by [29]. Splash impingement regime is employed in the present work.

Turbulence is modeled by the renormalization group RNG k-ε, and the model used for NOx formation is based on thermal mechanism, their details and validation are available in the literature [30, 31], also the details of the soot model are available in [31].

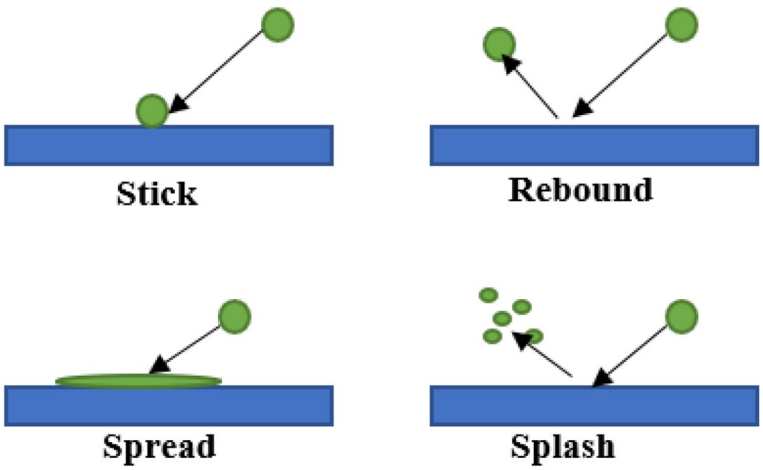

Fig. 6 Surface impingement regimes

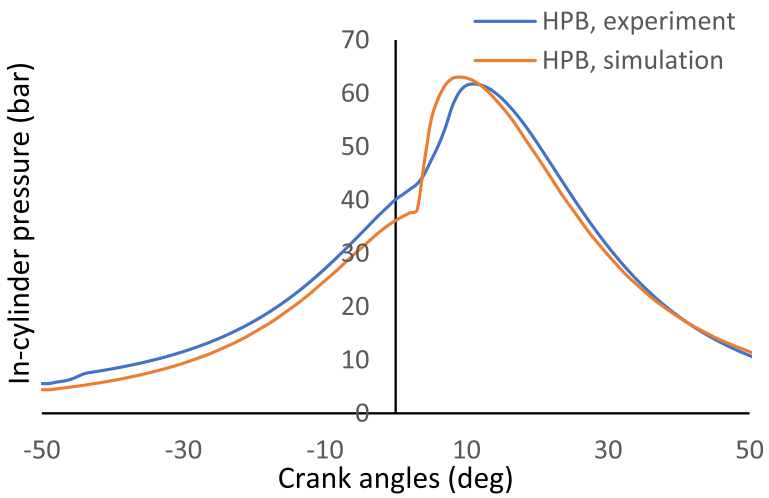

Fig. 7 Average in-cylinder pressure

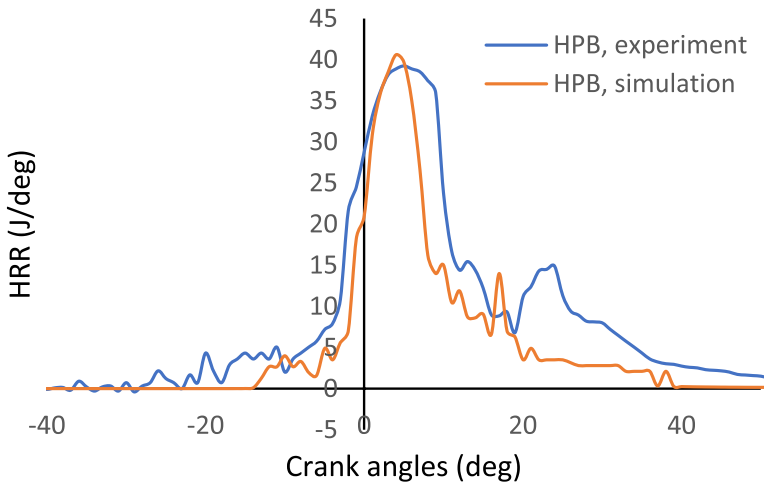

Fig. 8 Heat release rate

An experimental test is conducted on the diesel engine with a hemispherical piston bowl (HPB) and fueled with conventional diesel fuel. Figures 7 and 8 show the comparison of average in-cylinder pressure, as well as heat release rate (HRR) plots at 1500 rpm of engine speed; a good agreement is attained between the computational results and experimental results but, there is a deviation in the peak pressure value by about 1.7%, in addition to a deviation in the first peak of HRR by about 2.4%.

Results and discussion

The effect of piston bowl shape

Figure 9 shows the mean in-cylinder pressure and heat release rate (HRR) versus crank angles (CA) for the diesel-fueled engine with hemispherical piston bowl (HPB), toroidal piston bowl (TPB), and rectangular piston bowl (RPB). In the case of RPB, the pressure deviation is observed from the beginning of the compression

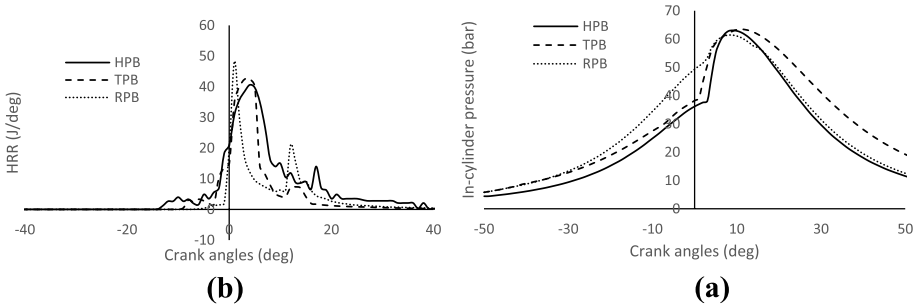

Fig. 9 **a** Mean in-cylinder pressure and **b** heat release rate at different piston bowl shapes

of charge inside the engine cylinder, where the pressure is significantly increased than other cases, indicating a non-smooth start. The two cases of HPB and TPB are closely similar, but the area under the pressure curve on the right-hand side for TPB is larger than other cases, which indicates that the diesel engine with TPB gives the largest network done, where the network done (W) by the engine is determined by the following equation:

$$W = \int_{TDC}^{BDC} PdV$$

Where P is the pressure and V is the volume.

Combustion in diesel engine occurs in two phases, namely pre-mixed and diffusion. The pre-mixed phase is responsible for the rapid combustion, whereas the diffusion phase begins after the rapid combustion, which is responsible for any change that takes place in the temperature and pressure inside the cylinder, and it can be controlled through the mixing of fuel with air [32–34]. From this context, the formation of the first peak in the HRR plot is due to the pre-mixed combustion phase, and its greater width indicates a good mixing and a large quantity of fuel is consumed during this phase. The presence of the second peak in HRR plot is a consequence of the diffusion combustion phase, and its size indicates the amount of fuel consumed during this phase. It is observed in the case of RPB that the first peak of the HRR plot appears thin and the second peak is larger than other cases, this indicates poor mixing which leads to higher emission concentrations.

As shown in Fig. 10, the vector plots refer to turbulent regions being formed inside the toroidal piston bowl (TPB), which resulted in better combustion characteristics and lower concentrations of soot emission. Figure 11 shows the emission development of carbon monoxide (CO), unburnt hydrocarbons (UHC) and nitric oxide (NO) inside the three shapes of piston bowl. It is observed that the emission concentrations of the three shapes stabilized at 55° CA, where the emission concentrations from TPB and HPB converged on each other. The emissions from RPB are higher than TPB and HPB due to the poor mixing. The higher nitric oxide that is exhausted from the RPB may be due to the higher spatial temperature, as seen in Fig. 10.

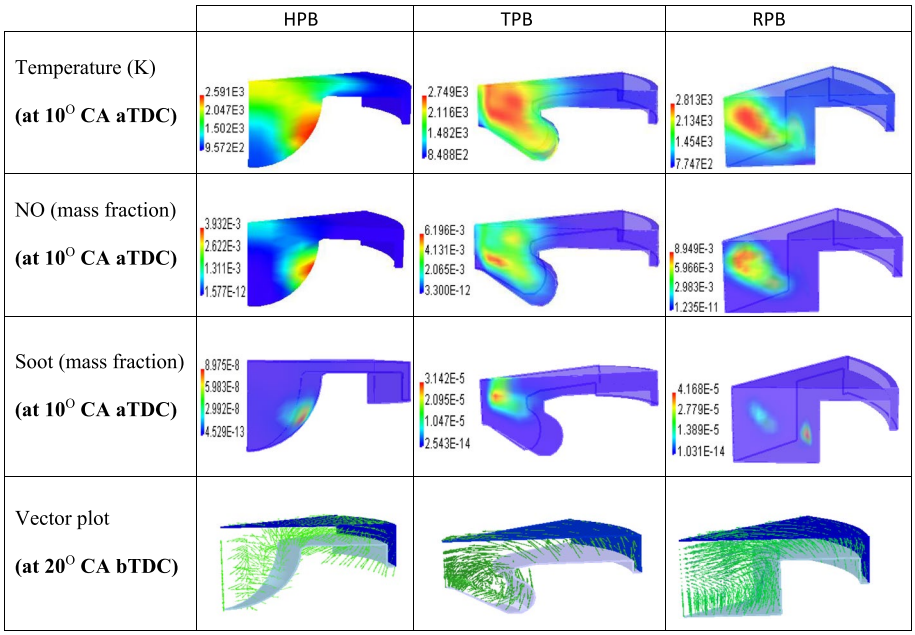

Fig. 10 Spatial distributions of temperature, NO and soot emission as well as vector plots inside different piston bowl shapes

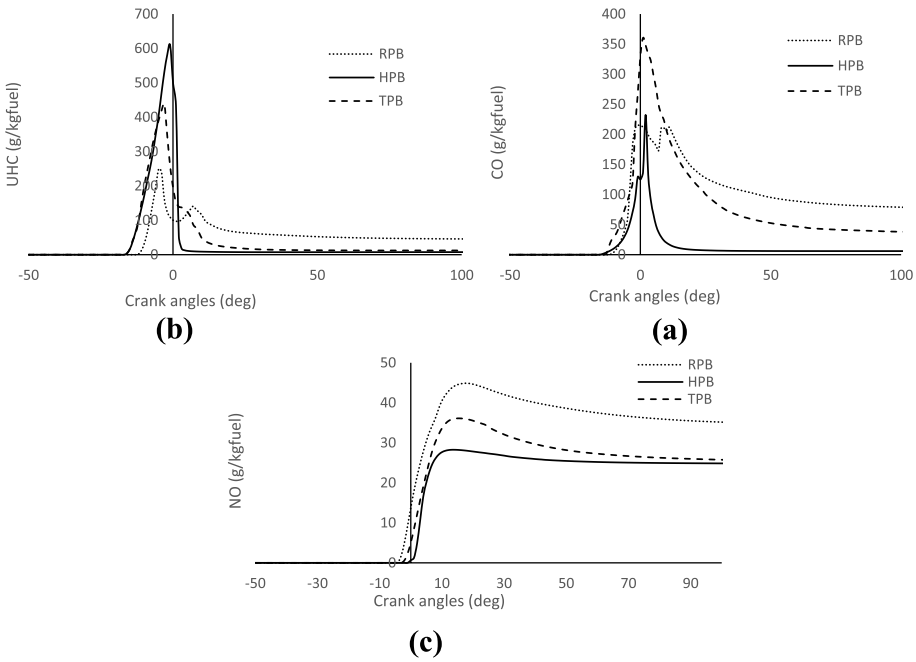

Fig. 11 Emission development of **a** carbon monoxide, **b** unburnt hydrocarbon, and **c** nitric oxide inside the three shapes of piston bowl

The effect of biodiesel fuel

Diesel engine with hemispherical piston bowl (HPB) is taken into consideration for comparing the combustion and emission of biodiesel and conventional diesel fuels. As

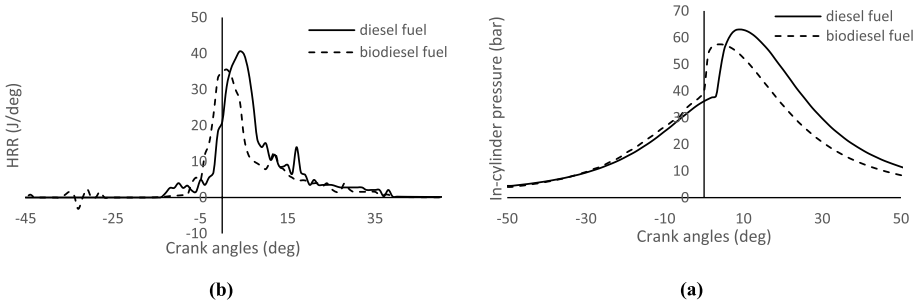

Fig. 12 Comparison of diesel and biodiesel fuels in terms of **a** in-cylinder pressure and **b** heat release rate

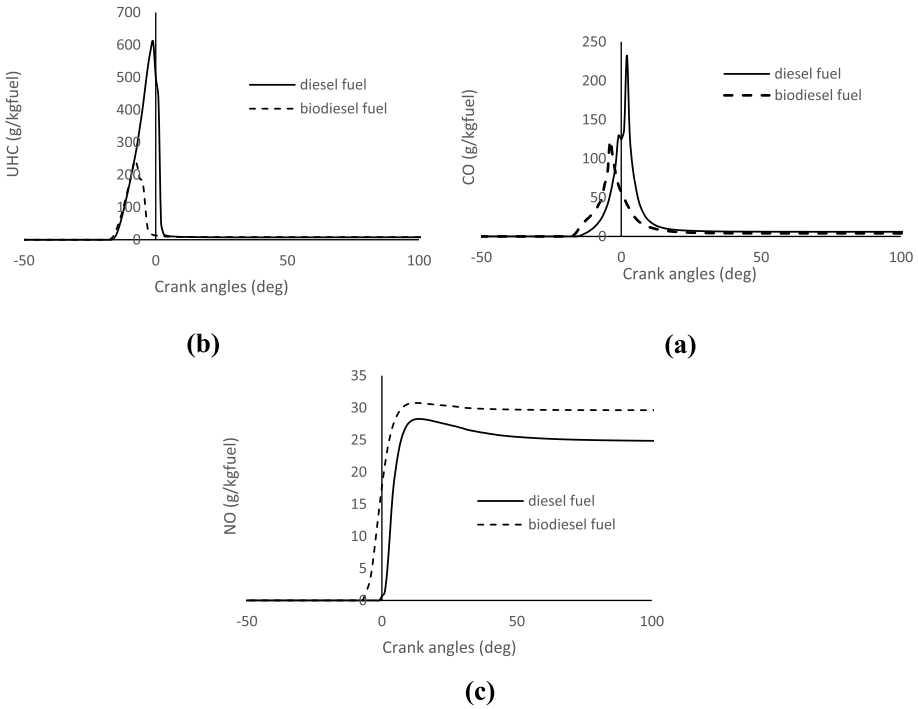

Fig. 13 Comparison of diesel and biodiesel fuels in terms of **a** carbon monoxide, **b** unburnt hydrocarbon, and **c** nitric oxide emissions

shown in Fig. 12, the rapid combustion stage of biodiesel fuel began earlier than conventional diesel fuel by about 5° CA, indicating that the biodiesel fuel has a shorter ignition delay period than diesel fuel. The shorter ignition delay period of biodiesel is due to its higher cetane number. The in-cylinder peak pressure of diesel fuel is about 5.4 bar higher than that of biodiesel fuel, this is due to the quantity of diesel fuel injected into the combustion chamber during the pre-mixed combustion phase being higher than that of biodiesel fuel. Furthermore, the area under the pressure curve of diesel fuel on the right-hand side is higher than that of biodiesel, which indicates the net work done by the diesel-fueled engine is higher than that of biodiesel fuel. It is observed that the HRR of biodiesel fuel decreased by 18.88% compared to diesel fuel, because the lower heating value of biodiesel is 12.8% lower than diesel fuel, as shown in Tables 3 and 4.

Figure 13 shows a comparison between the emissions from conventional diesel and biodiesel fuels in terms of CO, UHC and NO emissions. The formation of CO and UHC emissions inside the engine cylinder are influenced by the fuel type, fuel atomization and turbulence. It's observed that the emissions of CO and UHC from biodiesel fuel are significantly reduced as compared to diesel fuel, despite the higher viscosity, higher density and lower atomization rate of biodiesel fuel. The reduction in CO and UHC emissions of biodiesel fuel is due to its oxygen content, which improves the combustion efficiency and stimulates the conversion of CO to CO_2 emissions. As shown in Fig. 13c, the concentration of nitric oxide stabilized at 55° CA, where its value increased in the case of biodiesel fuel by about 17.78% compared to conventional diesel fuel, and this increase is due to its content of oxygen and unsaturated fatty acids.

Figure 14 depicts the fuel spray development, where the jet core of biodiesel fuel appears thicker and longer than conventional diesel fuel due its higher viscosity. Moreover, the atomization and vaporization rate of conventional diesel fuel are much better than those of biodiesel fuel.

Conclusions

The combustion chamber geometry and fuel type have a significant impact on the combustion and emission characteristics of diesel engines. The effects of three configurations of piston bowl shape and soybean biodiesel fuel on a diesel engine combustion and emission are investigated at an engine speed of 1500 rpm. The considered piston bowl shapes are hemispherical, toroidal and rectangular piston bowls. The main conclusion points can be summarized as

1. The effects of piston bowl shapes

Fuel	Fuel spray development	
	at 10 CA bTDC	at TDC
Biodiesel fuel	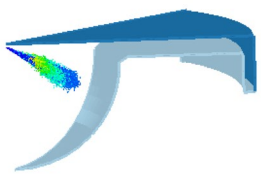	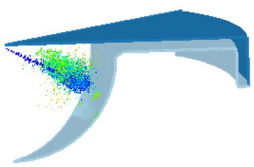
Diesel fuel	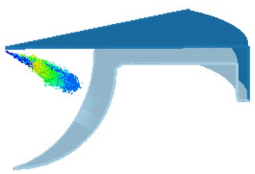	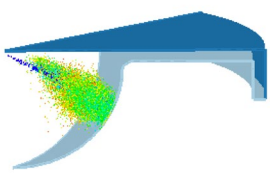

Fig. 14 Fuel spray development of diesel and biodiesel fuels

- In the case of a toroidal shape, the area under the in-cylinder mean pressure curve on the right-hand side is larger than in other cases, so the power delivered is a higher one.
- In the case of a rectangular shape, a non-smooth starting is observed, where a noticeable deviation in pressure occurs from the beginning of the compression of charge inside the engine cylinder.
- The toroidal shape provides a lower concentration of soot emission than other shapes, which turbulent regions with higher intensity are formed inside the toroidal piston bowl.
- The concentrations of CO, UHC, and NO emissions of the three shapes are stabilized at 55° CA, and it is observed that the emissions of the rectangular shape are higher than those of the toroidal and hemispherical shapes.

2. The effect of biodiesel fuel

- The rapid combustion stage of biodiesel fuel began earlier than the base diesel fuel by about 5° CA, which indicates that the biodiesel fuel has a shorter ignition delay period than diesel fuel.
- The in-cylinder mean peak pressure of diesel fuel is about 5.4 bar higher than that of biodiesel fuel.
- The heat release rate (HRR) of the biodiesel fuel decreased by 18.88% compared to diesel fuel, because the lower heating value of soybean biodiesel fuel is about 12.8% lower than diesel fuel.
- The oxygen content in biodiesel fuel enhanced the combustion efficiency and improved the conversion of CO into CO_2
- Due to the oxygen content in biodiesel fuel, the emissions of carbon monoxide (CO) and unburnt hydrocarbon are reduced, but the nitric oxide (NO) increased by about 17.78% at 55° CA, compared to diesel fuel.
- It is observed that the jet core of the biodiesel fuel appears thicker and longer than conventional diesel fuel due its higher viscosity so, the atomization rate of biodiesel fuel is lower than diesel fuel and may be enhanced by increasing the injection pressure.
- For optimization, preheating with exhaust gas recirculation (EGR) of biodiesel fuel contributes to reduce the emissions of nitrogen oxides (NO_x) and improve the atomization rate.
- The results of the present study indicate that biodiesel fuel is an environmentally friendly fuel which provide a lower concentration of harmful emissions as well as diesel engine with a toroidal piston bowl enhanced the turbulence intensity, which results in higher combustion efficiency and lower emissions.

Abbreviations

DI	Direct injection
CA	Crank angle
aTDC	After top dead center
bTDC	Before top dead center

CFD	Computational fluid dynamics
FAMEs	Fatty acid methyl esters
CO	Carbon monoxide
UHC	Unburnt hydrocarbon
NO	Nitric oxide
NO_x	Nitrogen oxides
CO_2	Carbon dioxide
HRR	Heat release rate (J/CA)
HPB	Hemispherical piston bowl
TPB	Toroidal piston bowl
RPB	Rectangular piston bowl

Acknowledgements
The authors would like to thank and acknowledge the support offered by the staff of Internal Combustion Engines Laboratory, Faculty of Engineering, Al-Azhar University, for their contributions to the experiments.

Authors' contributions
MKA conducted the numerical simulation, visualization, conceptualization, investigation, and wrote the manuscript. MMA supervised the laboratory experiments and structured. AME conducted the laboratory experiments, edited, read, and reviewed the final manuscript. All authors read and approved the final manuscript.

Authors' information
MKA is a researcher at the Mechanical Engineering Department, Faculty of Engineering, Al-Azhar University. MMA is currently a professor of internal combustion engines at the Mechanical Engineering Department, Faculty of Engineering, Al-Azhar University. AME is an assistant professor at the Mechanical Engineering Department, Faculty of Engineering, Al-Azhar University.

Funding
The authors declare that they did not receive any specific grant from funding agencies in the public, commercial, or not-for-profit sectors.

Availability of data and materials
The data used in the present study are available on request.

Declarations

Ethics approval and consent to participate
Not applicable.

Consent for publication
Not applicable.

Competing interests
The authors declare that they have no competing interests.

Received: 17 August 2022 Accepted: 31 October 2022
Published online: 12 November 2022

References

1. Reitz RD, Rutland CJ (1995) Development and testing of diesel engine CFD models. Progress Energy Combust Sci 21:173–196. https://doi.org/10.1016/0360-1285(95)00003-Z
2. Heywood JB (2018) Internal combustion engine fundamentals. McGraw-Hill Education, New York
3. Mikalsen R, Roskilly AP (2009) A computational study of free-piston diesel engine combustion. Appl Energy 86:1136–1143. https://doi.org/10.1016/j.apenergy.2008.08.004
4. Kouremenos DA, Rakopoulos CD, Hountalas DT (1997) Multi-zone combustion modeling for the prediction of pollutants emissions and performance of DI diesel engines. SAE Trans 106:940–957. https://doi.org/10.4271/970635
5. Jayashankara B, Ganesan V (2010) Effect of fuel injection timing and intake pressure on the performance of a DI diesel engine – a parametric study using CFD. Energ Conver Manage 51:1835–1848. https://doi.org/10.1016/j.enconman.2009.11.006
6. Peng Z, Liu B, Wang W, Lipeng L (2011) CFD investigation into diesel PCCI combustion with optimized fuel injection. Energies 4:517–531. https://doi.org/10.3390/en4030517
7. Abdul Gafoor CP, Gupta R (2015) Numerical investigation of piston bowl geometry and swirl ratio on emission from diesel engines. Energ Conver Manage 101:541–551. https://doi.org/10.1016/j.enconman.2015.06.007
8. Rakopoulos CD, Kosmadakis GM, Pariotis EG (2010) Investigation of piston bowl geometry and speed effects in a motored HSDI diesel engine using a CFD against a quasi-dimensional model. Energ Conver Manage 51:470–484. https://doi.org/10.1016/j.enconman.2009.10.010
9. Jaichandar S, Senthil Kumar P, Annamalai K (2012) Combined effect of injection timing and combustion chamber geometry on the performance of a biodiesel fueled diesel engine. Energy 47:388–394. https://doi.org/10.1016/j.energy.2012.09.059

10. Saito T, Daisho Y, Uchida N, Ikeya N (1986) Effects of combustion chamber geometry on diesel combustion. SAE Trans 95(793):803. https://doi.org/10.4271/861186
11. Rajamani V, Schoenfeld S, Dhongde A (2012) Parametric analysis of piston bowl geometry and injection nozzle configurations using 3D CFD and DoE. SAE paper 2012-01-0700. https://doi.org/10.4271/2012-01-0700
12. Thomas TP, Birney DM, Auld DL (2013) Optimizing esterification of safflower, cottonseed, castor and used cottonseed oils. Ind Crop Prod 41:102–106. https://doi.org/10.1016/j.indcrop.2012.03.023
13. Candeia RA, Silva MCD, Filho JRC, Brasilino MGA, Bicudo TC, Santos IMG, Souza AG (2009) Influence of soybean biodiesel content on basic properties of biodiesel–diesel blends. Fuel 88:738–743. https://doi.org/10.1016/j.fuel.2008.10.015
14. Wazilewski WT, Bariccatti RA, Martins GI, Secco D, Souza SNM, Rosa HA, Chaves LI (2013) Study of the methyl crambe (Crambe abyssinica Hochst) and soybean biodiesel oxidative stability. Ind Crop Prod 43:207–212. https://doi.org/10.1016/j.indcrop.2012.07.046
15. Elumalai PV, Dash SK, Parthasarathy M, Dhineshbabu NR, Balasubramanian D, Coa DN, HaiTruong T, Le AT, Hoang AT (2022) Combustion and emission behaviors of dual-fuel premixed charge compression ignition engine powered with n-pentanol and blend of diesel/waste tire oil included nanoparticles. Fuel 324:124603. https://doi.org/10.1016/j.fuel.2022.124603
16. Nachippan NM, Parthasarathy M, Elumalai PV, Backiyaraj A, Balasubramanian D, Hoang AT (2022) Experimental assessment on characteristics of premixed charge compression ignition engine fueled with multi-walled carbon nanotube-included Tamanu methyl ester. Fuel 323:124415. https://doi.org/10.1016/j.fuel.2022.124415
17. Elumalai PV, Parthasarathy M, Hariharn V, Jayakar J, Iqbal SM (2021) Evaluation of water emulsion in biodiesel for engine performance and emission characteristics. J Therm Anal Calorimetry 147:4285–4301. https://doi.org/10.1007/s10973-021-10825-z
18. Ng HK, Gan S, Ng JH, Pang KM (2013) Simulation of biodiesel combustion in a light -duty diesel engine using integrated compact biodiesel-diesel reaction mechanism. Appl Energy 102:1275–1287. https://doi.org/10.1016/j.apenergy.2012.06.059
19. Lin B-F, Huang J-H, Huang D-Y (2009) Experimental study of the effects of vegetable oil methyl ester on DI diesel engine performance characteristics and pollutant emissions. Fuel 88:1779–1785. https://doi.org/10.1016/j.fuel.2009.04.006
20. Canakcı M (2007) Combustion characteristics of a turbocharged DI compression ignition engine fueled with petroleum diesel fuels and biodiesel. Bioresour Technol 98:1167–1175. https://doi.org/10.1016/j.biortech.2006.05.024
21. Al EL-S, He Z, Hassan H, Balasubramanian D (2020) Improvement of combustion and emission characteristics of a diesel engine working with diesel/jojoba oil blends and butanol additive. Fuel 279:118433. https://doi.org/10.1016/j.fuel.2020.118433
22. Senthilkumar PB, Parthasarathy M, Nagarajan R, Murgunachiappan N, Elumalai PV, Varaprasad BH (2022) The effect of thermal degradation and thermogravimetric analysis on pyrolysis oil production from waste milk packet for CI engine application. J Therm Anal Calorimetry 147:9677–9691. https://doi.org/10.1007/s10973-022-11226-6
23. Sivakandhan C, Elumalai PV, Murugan M, Saravanan A, Ranjit PS, Varaprasad B (2022) Effects on MnO_2 nanoparticles behavior of a sardine oil methyl ester operated in thermal barrier coated engine. J Therm Anal Calorimetry 147:8919–8931. https://doi.org/10.1007/s10973-021-11132-3
24. Patel A, Kong S, Reitz RD (2004) Development and validation of a reduced reaction mechanism for HCCI engine simulations. SAE Technical Paper 2004-01-0558. https://doi.org/10.4271/2004-01-0558
25. Jung JW, Lim YC, Suh HK (2020) A study on the mechanism reduction and evaluation of biodiesel with the change of mechanism reduction factors. Proc IMechE Part D: J Automobile Eng 234:3398–3413. https://doi.org/10.1177/0954407020931694
26. Beale JC, Reitz RD (1999) Modeling spray atomization with the Kelvin-Helmholtz/Rayleigh-Taylor hybrid model. Atomization Sprays 9:623–650. https://doi.org/10.1615/AtomizSpr.v9.i6.40
27. Su TF, Patterson MA, Reitz RD, Farrell PV (1996) Experimental and Numerical Studies of High Pressure Multiple Injection Sprays. SAE T Trans 105:1281–1292. https://doi.org/10.4271/960861
28. Bai C, Gosman AD (1996) Mathematical modeling of wall films formed by impinging sprays. SAE Trans 105:782–796. https://doi.org/10.4271/960626
29. Han Z, Xu Z, Trigui N (2000) Spray/wall interaction models for multidimensional engine simulation. Int J Engine Res 1:127–146. https://doi.org/10.1243/1468087001545308
30. Yakhot V, Orszag SA (1986) Renormalization group analysis of turbulence. I. Basic Theory. J Scientific Comput 1:3–51. https://doi.org/10.1007/BF01061452
31. Hiroyasu H, Kadota T (1976) Models for Combustion and Formation of Nitric Oxide and Soot in DI Diesel Engines. SAE Tech 85:513–526. https://doi.org/10.4271/760129
32. Dhuchakallaya I, Watkins AP (2010) Application of spray combustion simulation in DI diesel engine. Appl Energy 87:1427–1432. https://doi.org/10.1016/j.apenergy.2009.08.029
33. Leung DYC, Luo Y, Chan TL (2006) Optimization of exhaust emissions of a diesel engine fuelled with biodiesel. Energy Fuel 20:1015–1023. https://doi.org/10.1021/ef050383s
34. Sahoo PK, Das LM (2009) Combustion analysis of Jatropha, Karanja and Polanga based biodiesel as fuel in a diesel engine. Fuel 88:994–999. https://doi.org/10.1016/j.fuel.2008.11.012

Publisher's Note